

## Studies of phase turbulence in the one-dimensional complex Ginzburg-Landau equation

Alessandro Torcini, Helge Frauenkron, and Peter Grassberger  
*Theoretical Physics, Wuppertal University, D-42097 Wuppertal, Germany*  
 (Received 2 July 1996; revised manuscript received 2 December 1996)

The phase-turbulent (PT) regime for the one-dimensional complex Ginzburg-Landau equation (CGLE) is carefully studied, in the limit of large systems and long integration times, using an efficient integration scheme. Particular attention is paid to solutions with a nonzero phase gradient. For fixed control parameters, solutions with conserved average phase gradient  $\nu$  exist only for  $|\nu|$  less than some upper limit. The transition from phase to defect turbulence happens when this limit becomes zero. A Lyapunov analysis shows that the system becomes less and less chaotic for increasing values of the phase gradient. For high values of the phase gradient a family of nonchaotic solutions of the CGLE is found. These solutions consist of spatially periodic or aperiodic waves traveling with constant velocity. They typically have incommensurate velocities for phase and amplitude propagation, showing thereby a type of quasiperiodic behavior. The main features of these traveling wave solutions can be explained through a modified Kuramoto-Sivashinsky equation that rules the phase dynamics of the CGLE in the PT phase. The latter explains also the behavior of the maximal Lyapunov exponents of chaotic solutions. [S1063-651X(97)08604-2]

PACS number(s): 05.45.+b, 47.27.Cn, 47.27.Eq

### I. INTRODUCTION

The complex Ginzburg-Landau equation (CGLE) plays a fundamental role in the study of spatially extended systems. It describes the dynamics of a generic spatially extended system that undergoes a Hopf bifurcation from a stationary to an oscillatory state. Sufficiently close to the bifurcation point, any such system can be described by the CGLE [1]. For a review of experimental systems described by the CGLE see [2].

In the present paper we discuss only the CGLE in one spatial dimension. Even though this lacks important features of the CGLE in higher dimensions, it displays a variety of chaotic and stationary regimes for different values of control parameters. Recently, Shraiman *et al.* [3] and Chaté [4] have provided a careful description of these regimes. In particular, four different chaotic states have been identified: the phase-turbulent (PT), the defect-turbulent (DT), the bichaotic, and the spatiotemporal intermittent regime [4]. The fundamental states are the PT and the DT regimes. The bichaotic state is characterized by the fact that PT or DT chaos can arise, depending on the initial conditions — while DT chaos or stable (periodic) solutions can appear in the intermittent region. The PT and DT phases have been the object of several detailed studies [3,5–9].

Let us write the one-dimensional CGLE as

$$A_t = (1 + ic_1)A_{xx} + A - (1 - ic_3)|A|^2 A, \quad (1)$$

where the parameters  $c_1$  and  $c_3$  are real positive numbers, while  $A(x,t) = \rho(x,t)\exp[i\psi(x,t)]$  is a complex field of amplitude  $\rho$  and phase  $\psi$ . Equation (1) reduces in the limit  $(c_1, c_3) \rightarrow (\infty, \infty)$  to the integrable nonlinear Schrödinger equation, an equation well known to admit soliton-like solutions [10]. In the opposite limit,  $(c_1, c_3) \rightarrow (0, 0)$ , the real Ginzburg-Landau equation will be recovered, an equation related to symmetry-breaking instabilities of nonoscillatory type [1].

Equation (1) admits plane-wave solutions of the form

$$A_0(x,t) = \sqrt{1 - k^2} \exp[i(kx - \Omega_0 t)], \quad (2)$$

where  $\Omega_0 = -c_3 + (c_1 + c_3)k^2$ . Below the so-called Benjamin-Feir (BF) line defined by  $c_3 = 1/c_1$  these solutions are linearly stable provided  $k^2 < (1 - c_1 c_3) / [2(1 + c_3^2) + 1 - c_1 c_3]$  [11]. Outside this “Benjamin-Feir band,” one has an Eckhaus instability against long-wavelength modes. Slightly below the BF line one finds multistability; i.e., the final solution depends on the initial conditions [4]. Above it, i.e., for  $c_3 c_1 > 1$ , all plane-wave modes are unstable. The latter is the region we are interested in.

For generic (not necessarily periodic) solutions, the *average* phase gradient is defined as

$$\nu = \frac{1}{L} \int_0^L dx \partial_x \psi(x,t), \quad (3)$$

where  $L$  is the system size (we assume periodic boundary conditions  $A(x+L,t) = A(x,t)$  throughout this paper, unless stated differently). The PT phase is defined as that regime where  $\nu$  is conserved [5]. It is encountered just above the BF line (i.e., for  $c_3 > 1/c_1$ ). It is a state where the chaotic behavior of the field is essentially ruled by the phase dynamics. The amplitude, always bounded away from zero for Eq. (3) to make sense, shows small fluctuations.

This is different in the DT regime in which the amplitude-dynamics becomes essential [3,5,6]. Large amplitude oscillations are observed in this phase, which occasionally drive  $\rho(x,t)$  down to zero. Events where this happens are called defects. At a defect, the phase is of course no longer defined, and the appearance of a defect implies that the phase difference  $\psi(x + \epsilon, t) - \psi(x - \epsilon, t)$  jumps by  $\pm 2\pi$ . Thus  $\nu$  is no longer conserved.

The transition from the PT to the DT regime happens at a line  $L_1$  in the  $(c_1, c_3)$  plane. To locate this transition precisely [3,9], one needs some order parameter that allows one

to distinguish the two phases. Several parameters have been proposed recently: the density of defects, the phase and amplitude correlation lengths, and the Kaplan-Yorke dimension [7–9]. The first-order parameter introduced to identify the two phases is the defect density  $\delta_D$  [3]. Its value is  $>0$  in the DT regime, while it vanishes when approaching the PT phase [3,9]. Presenting other suitable order parameters will be one of the aims of the present paper.

In the PT regime, all observables depend of course on the value of  $\nu$ , as ergodicity is broken in this phase. Nevertheless, in the literature only few studies have been devoted to solutions with  $\nu \neq 0$  [12,13]. Filling this gap is the second goal of the present paper. It will be shown that most observables depend indeed rather strongly and systematically on  $\nu$ .

Since our study is mostly numerical, we need an efficient integration routine. We found that a scheme, similar to but more efficient than the one introduced in [15], gave excellent results. This scheme is introduced in the next section and compared with the usual pseudospectral codes. In Sec. III the transition from phase to defect turbulence is investigated with the help of an order parameter. A Lyapunov analysis for the solutions with  $\nu \neq 0$  is reported in Sec. IV together with a detailed characterization of the observed stable solutions. In Sec. V it is shown how a modified Kuramoto-Sivashinsky equation for the phase is able to reproduce the main features of the dynamics of the considered solutions of the CGLE. Our results are summarized in Sec. VI.

## II. INTEGRATION SCHEME

The algorithm applied in this work is an operator splitting scheme similar to the well known ‘‘leap frog’’ algorithm for ordinary differential equations [this should not be confused with the ‘‘staggered leap frog’’ [14] for partial differential equations (PDE’s)]. This algorithm is based on the fact that the dynamics consists of two independent terms, one nonlinear but local and the other nonlocal but linear, each of which by itself can be easily integrated. In the present case, this splitting is chosen as

$$\frac{\partial A}{\partial t} = \mathcal{N}A + \mathcal{L}A \quad (4)$$

with

$$\mathcal{N}A = A - (1 - ic_3)|A|^2A, \quad \mathcal{L}A = (1 + ic_1)\frac{\partial^2 A}{\partial x^2}. \quad (5)$$

For a small time step  $\tau$ , the formal solution  $A(t) = e^{(N+\mathcal{L})t}A(0)$  of Eq. (4) is then approximated by means of the Trotter formula

$$e^{(N+\mathcal{L})\tau} \approx e^{N\tau/2} e^{\mathcal{L}\tau} e^{N\tau/2} + O(\tau^3). \quad (6)$$

For a finite time  $t = n\tau, n \gg 1$ , we can lump together  $n-1$  half steps and arrive at

$$e^{(N+\mathcal{L})t} \approx e^{N\tau/2} [e^{\mathcal{L}\tau} e^{N\tau}]^{n-1} e^{\mathcal{L}\tau} e^{N\tau/2}. \quad (7)$$

Notice that we refrain from giving here a formal error estimate. For a chaotic system, the error will of course increase

exponentially, and the exponent will depend on the maximal Lyapunov exponent  $\lambda$ : roughly we expect  $\delta A(t) \sim e^{c\lambda\tau^2}$ , where  $c$  is the constant in the  $O(\tau^3)$  correction in Eq. (6).

Solving the nonlinear evolution  $e^{N\tau}$  is easy, by considering amplitude and phase separately. We first find

$$\rho_1(x, t + \tau) \equiv [e^{N\tau}\rho](x, t) = \{e^{-2\tau}[1/\rho(x, t)^2 - 1] + 1\}^{-1/2}. \quad (8)$$

Inserting this into the equation for the phase, the latter can also be solved exactly to obtain

$$\begin{aligned} \psi_1(x, t + \tau) &\equiv [e^{N\tau}\psi](x, t) \\ &= \psi(x, 0) + c_3\{\tau + \ln[\rho(x, t)/\rho_1(x, t + \tau)]\}. \end{aligned} \quad (9)$$

A nontrivial problem appears only for the solution  $e^{\mathcal{L}t}$  of the linear part since this is nonlocal. It is only here that our algorithm deviates from previous applications of the leap frog algorithm to PDE’s [16–20]. In these papers, the solution of the nonlocal part was performed in Fourier space. This means that two Fourier transformations have to be performed for each integration step. It leads to what will be called the pseudospectral method in the following. In spite of the speed of fast Fourier transform (FFT) algorithms, it can be quite time consuming. It can also lead to intolerable round-off errors, which was the main reason in [15] to perform this step by integrating with the Greens function of  $\mathcal{L}$ . More precisely, let us denote by  $K(x, t)$  the solution of

$$\partial K / \partial t = \mathcal{L}K \quad (10)$$

with initial condition  $K(x, 0) = \delta(x)$ . For the present case it is simply

$$K(x, \tau) = \sqrt{\frac{\beta}{\pi}} e^{-\beta_r x^2} [\cos(\beta_i x^2) - i \sin(\beta_i x^2)] \quad (11)$$

with  $\beta = \beta_r - i\beta_i = [4\tau(1 + ic_1)]^{-1}$ . Then

$$[e^{\mathcal{L}\tau}A](x, t) = \int d\xi K(\xi, \tau) A(x - \xi, t). \quad (12)$$

Since  $K(\xi, \tau)$  can be computed numerically and stored once at the beginning, the algorithm essentially involves one convolution for each time step.

In practice, space has of course to be discretized as well. Let us denote  $A_i(t) = A(i\Delta, t)$ , where  $\Delta$  is the resolution of the spatial grid. The most straightforward approach (used indeed in [15]) would seem to start from Eq. (12), with the integral simply replaced by a finite sum over the central site plus its  $2N$  nearest neighbors, which would lead to

$$[e^{\mathcal{L}\tau}A]_i(t) \approx \sum_{j=-N}^N K(j\Delta, \tau) A_{i-j}(t). \quad (13)$$

But this is not the optimal discrete approximation to Eq. (12). To obtain a more precise one, we first notice that since  $e^{\mathcal{L}\tau}A$  is a linear operator symmetric under translations and reflections  $x \rightarrow -x$ , we can write any lattice approximation of it as

$$[e^{\mathcal{L}\tau}A]_i(t) \approx \sum_{j=0}^N K_j [A_{i-j}(t) + A_{i+j}(t)], \quad (14)$$

with unknown coefficients  $K_j$ . Next we observe that we can decompose  $A(x,t)$  into Fourier modes. Let us assume that a good approximation is obtained by a superposition of  $2N+1$  modes  $e^{ik\alpha x}$  with  $k = -N, \dots, N$ , and  $\alpha$  some yet unspecified positive constant. We then can determine the  $K_j$  such that it gives the exact evolution on these modes. A straightforward calculation shows that this implies

$$K_0 + 2 \sum_{j=1}^N K_j \cos(j\Delta k \alpha) = e^{-(1+ic_1)tk^2\alpha^2} \mathbf{V}k = 0, \dots, N. \quad (15)$$

Finally, the value of  $\alpha$  is chosen such that the  $L_2$  norm  $\{|K_0|^2 + 2\sum_{j>0}|K_j|^2\}^{1/2}$  of  $K$  is minimal. With this choice, we hopefully minimize the effect of the neglected modes.

In the limit  $N \rightarrow \infty$ , the optimal set of Fourier modes are those with  $\alpha = 2\pi/\Delta$ , and the above scheme should give identical results (up to round-off errors) as the pseudospectral method obtained by applying a discrete FFT to  $A_i = \mathcal{L}A$  and integrating it in Fourier space. Thus the error committed in our method with finite  $N$  cannot be smaller than the error committed by the FFT method, and it should tend towards it for  $N \rightarrow \infty$ .

In order to compare the precision of our algorithm with that of the pseudospectral code, we have evaluated the mean square errors accumulated during a fixed total integration time  $T=1$  for different values of the spatial resolution  $\Delta$  and of the number  $N$  of convolution channels. In all simulations reported below, the time step and the parameter of the CGLE have been  $\tau=0.05$ ,  $c_1=3.5$ , and  $c_3=0.9$ . The errors have been estimated by measuring the distance (in  $L_2$  norm) between an orbit obtained by the algorithm to be tested (“test orbit”) and a reference orbit obtained by the pseudospectral method. In order to reduce statistical fluctuations, the reference orbit was integrated for a time  $\gg T$ , the test orbit was synchronized to it periodically at times  $t=mT$ ,  $m=1,2,\dots$ , and the distances building up during the intervals  $mT < t < (m+1)T$  were averaged over.

For estimating the error due to time discretization, we used a reference orbit with the same  $\Delta$  as the test orbit, but with four times smaller  $\tau$ . This error is the same for our algorithm and for a standard pseudospectral code. It is indicated in Fig. 1 by a dashed line. To estimate the space discretization error, the reference orbit had the same  $\tau$ , but half the value of  $\Delta$  (and, in effect,  $N=\infty$ ). Results concerning space discretization errors are reported in Fig. 1 for different  $\Delta$  and different  $N$ . From these data we can draw the following conclusions: (i) For all studied values of  $\tau$  and  $\Delta$ , the time discretization had a much bigger effect than space discretization. We could of course have used a smaller value of  $\tau$  (or a larger  $\Delta$ ) to avoid this, but our choices were motivated by previous simulations [3,4,7,9]. Nevertheless, we propose that future simulations should use finer time and/or coarser space grids. (ii) The convergence of the spatial truncation errors with  $N$  is quite fast. Typically, the error is less than twice the error of the FFT code for  $N \geq 20$ . This is in contrast to the scheme of [15], where  $N$  had to be chosen

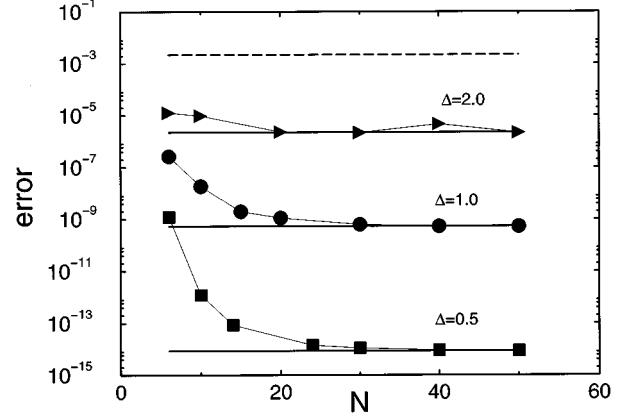


FIG. 1. Mean square errors due to space discretization and truncation of the convolution for our algorithm (symbols), and due to space discretization for a time splitting pseudospectral code (solid lines). The dashed line shows the errors due to the time discretization (they are the same for both algorithms, and independent of the spatial discretization). All the data refer to  $c_1=3.5$ ,  $c_3=0.9$ ,  $\tau=0.05$ , and  $N=1024$ . The results for our algorithm are reported for several values of the number of convolution channels  $N$ . The simulations were done with double precision, whence the roundoff errors are at  $\sim 10^{-15}$ .

larger than  $\approx 60$ . Due to the large time discretization error, we could indeed safely use  $N=10$ . (iii) The FFT code needs a CPU time per mesh point that increases logarithmically with the number  $L/\Delta$  of mesh points, while our algorithm is essentially linear in  $N$ . Using the FFT routine C06ECF of the NAG library, the ratio between the CPU times needed by our algorithm and the pseudospectral one was  $0.24N/\ln(L/\Delta)$ . For typical simulations reported in this paper ( $N=10, L=1024-4096, \Delta=1/2$ ), this ratio is  $\approx 0.25-0.3$ . Thus our algorithm is indeed considerably faster than the pseudospectral one.

### III. ORDER PARAMETERS AND THE PT-DT TRANSITION

To obtain configurations with nonvanishing  $\nu$ , we used several different initial conditions. A first choice was

$$A_k(t=0) = e^{i\nu k \Delta} + (r_k + ip_k), \quad (16)$$

with  $r_k$  and  $p_k$  random numbers uniformly distributed in  $[-0.1, 0.1]$ . Notice that the randomness is needed to break spatial translation invariance. Another ansatz was

$$A_k(t=0) = e^{i\nu k \Delta + s_k} \rho_k(0), \quad (17)$$

where  $\rho_k(0)$  was uniformly distributed in  $[0.2, 1.2]$ , and  $s_k \in [-0.01, 0.01]$ . Finally, in a third type of initial condition we introduced also long range correlations in the amplitude,

$$\rho_k(0) = 0.95\rho_{k-1}(0) + q_k, \quad q_k \in [-0.05, 0.05]. \quad (18)$$

All these initial conditions give consistent final results: in the regime identified as phase turbulent by previous authors,  $\nu$  is indeed conserved for sufficiently small initial values. However, for each pair  $(c_1, c_3)$  there exists an upper limit  $\nu_M$  above which defects arise in the system, leading finally to a phase gradient  $\nu \leq \nu_M$ . Therefore, defects will arise also

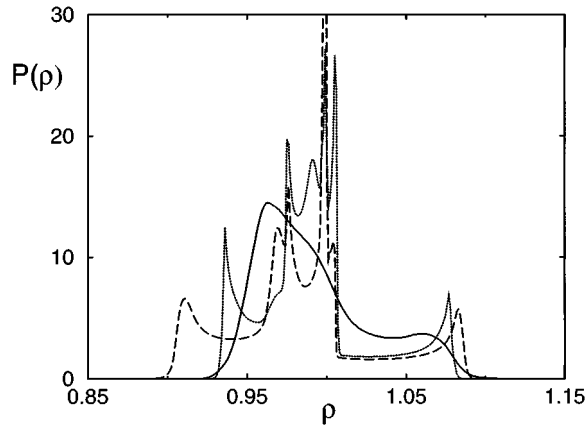


FIG. 2. Probability distribution  $P(\rho)$  for  $c_3=0.6$ ,  $c_1=3.5$  and for three different values of  $\nu$ : 0.015 (solid line), 0.046 (dotted line), and 0.098 (dashed line).

in the PT regime, provided that the value of  $\nu$  is sufficiently high. The distribution  $P(\rho)$  of the amplitude in the statistically stationary state becomes in general wider with increasing  $\nu$ , as shown in Fig. 2. In particular, the lower limit  $\rho_{\min}$  of its support decreases with  $\nu$ . But it seems that this decrease is discontinuous, so that  $\rho_{\min}$  cannot be used as a good order parameter (our conclusion has been drawn from the analysis of more than the 3 curves reported in Fig. 2). As pointed out in [12], we expect that the appearance of defects for solutions with  $\nu > \nu_M$ , in the PT regime, and for solutions with  $\nu=0$ , in the DT regime, will be due to the same mechanism. We will come back to this point later.

The dependence of  $\nu_M$  on  $c_3$  is plotted in Fig. 3 for  $c_1=3.5$ . This fixed value of  $c_1$  was chosen for ease of comparison with previous studies. We see an almost linear decrease, and  $\nu_M$  reaches zero exactly at the line  $L_1$  which marks the onset of DT (this was also seen in [12]).

Thus  $\nu_M$  can be used as order parameters to characterize the transition from phase to amplitude turbulence. From the

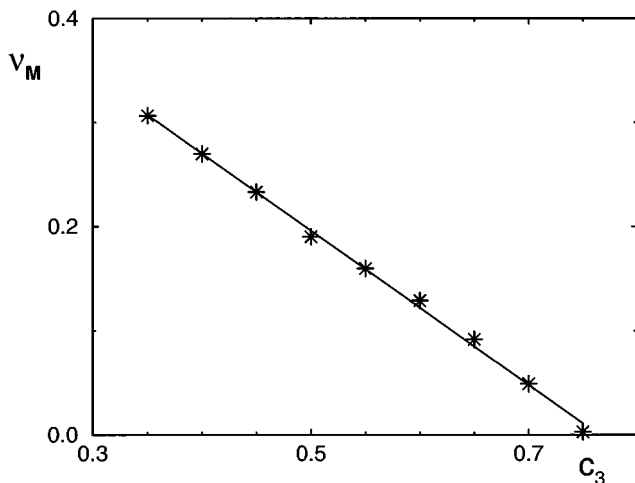


FIG. 3. Maximal phase gradient  $\nu_M$  as a function of the parameter  $c_3$  (asterisks). The solid line represents a linear fit for the  $\nu_M$  data. For each reported  $c_3$  value, we have considered from 50 to 70 distinct initial conditions with  $\nu > \nu_M$ , corresponding to a total integration time ranging from  $t=600\,000$  to  $t=10^6$ .

general theory of continuous phase transitions we would in general not expect a linear behavior of the order parameter as the transition is approached. Thus we should be suspicious that the linearity seen in Fig. 3 might give way to a power law for very small  $\nu_M$ .

In order to understand this better and to characterize better the transition between phase and defect turbulence (always concentrating on the value  $c_1=3.5$ , which we assume to be a generic point on the line  $L_1$ ), we performed several simulations with high statistics. For each value of  $c_3$  we performed  $\sim 50$ – $70$  simulations with  $\nu > \nu_M$  and with independent initial conditions, and followed them for  $\geq 10\,000$  time units (some simulations were followed even for  $> 10^5$  time units), unless a defect is found — in which case  $\nu$  is decreased and the simulation is repeated. We carefully checked that  $\nu_M$  did not depend on the system size by using systems with  $L$  ranging from 1024 to 4096. Nevertheless, the present simulations did not show any significant deviation from linearity in the dependence of  $\nu_M$  on  $c_3$ , and our best fit is

$$\nu_M \approx -(0.74 \pm 0.01)c_3 + 0.57 \pm 0.01. \quad (19)$$

From this we can estimate the critical value of  $c_3$  to be  $c_3^* = 0.76 \pm 0.03$ . Notice that the linearity of  $\nu_M$  agrees with a mean field description, since the critical exponent for the order parameter in cases without spontaneous symmetry breaking is 1.

Previous estimates of  $c_3^*$  (for the same value of  $c_1$ ) were all made by approaching the transition from the DT side. The defect density  $\delta_D$  was measured in [3,9] by counting how often the total phase difference  $\delta\psi(t) = \psi(x+L, t) - \psi(x, t)$  changed when going from  $t$  to  $t + \tau$ . Assuming a scaling law  $\delta_D \sim (c_3 - c_3^*)^\alpha$ , the authors of [3] found  $c_3^* \approx 0.77$  and  $\alpha \approx 2$ . In contrast,  $c_3^* = 0.74$  and  $\alpha \approx 6.8$  was found in [9] using a much higher statistics (iteration times up to  $10^7$  units,  $L=4096$  against  $L=1024$  in [3]). As mentioned in [9], the very large value of  $\alpha$  suggests that the data presumably do not follow a power law. Indeed, another extrapolation was also tried in [9], which gave  $c_3^* = 0.70$ . Thus our result quoted above is in good agreement with previous estimates, in view of the latter's uncertainties.

To obtain an independent estimate of  $c_3^*$  and of an eventual scaling exponent governing the approach from the DT side, we performed simulations (with  $\nu=0$ ) for several values  $c_3 \geq c_3^*$ . In these simulations we did not measure actual defects but *near* defects. More precisely, we made histograms of  $P(\rho)$  similar to the one shown in Fig. 2. A number of such histograms are shown in Fig. 4 [actually, the quantity shown in Fig. 4 is  $P(\rho)/(2\pi\rho)$ , i.e., the two-dimensional density]. We see much wider distributions than in Fig. 2, reflecting again the higher degree of chaos for  $\nu=0$ . From these histograms we can estimate the probabilities

$$w(\rho) = \int_0^\rho dx P(x) \quad (20)$$

to have an amplitude  $< \rho$ . We did this for several values of  $\rho$ , and plotted the results against  $c_3 - c_3^*$  in a log-log plot (see Fig. 5). We see a decent scaling law if  $c_3^*$

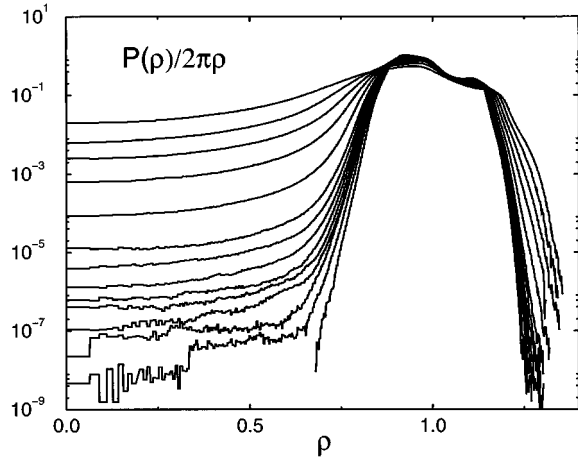


FIG. 4. Probability distributions  $P(\rho)$  similar to those shown in Fig. 2, but for  $\nu=0$ , divided by  $2\pi\rho$ , and shown on a logarithmic scale. For all curves  $c_1=3.5$ . From bottom to top, the values of  $c_3$  are 0.74, 0.746, 0.75, 0.752, 0.755, 0.758, 0.761, 0.765, 0.77, 0.783, 0.8, 0.82, 0.85, and 0.9. Except possibly for the lowest, all curves are in the DT regime. The simulations closest to  $c_3^*$  were done with  $L=4096$  and extended over  $>2 \times 10^5$  time units.

$=0.734 \pm 0.007$  (which we take as our best estimate of  $c_3^*$ ), with an exponent  $\approx 6.3$ . Our results confirm that the simulations performed in [9] should be considered definitely more reliable than those reported in [3]. This large exponent might, however, suggest that the data should not be described by a power law at all [9]. In that case, the true value of  $c_3^*$  could be considerably smaller and close to the ‘‘alternative’’ value 0.70 found in [9]. Thus the agreement with previous simulations and with Eq. (19) is as good as can be expected in view of these uncertainties.

In Fig. 4 it is seen that  $\rho_{\min}$  [the lower limit of the support of  $P(\rho)$ ] does not approach zero continuously as  $c_3 \rightarrow c_3^* - \epsilon$ . Instead, as  $c_3$  approaches  $c_3^*$  from below, it seems that  $\rho_{\min}$  jumps abruptly to 0 [21,23]. On the other hand, the two-dimensional density  $P(\rho)/(2\pi\rho)$  seems to be flat at  $\rho=0$ , for all  $c_3 > c_3^*$ . As a consequence, the distribu-

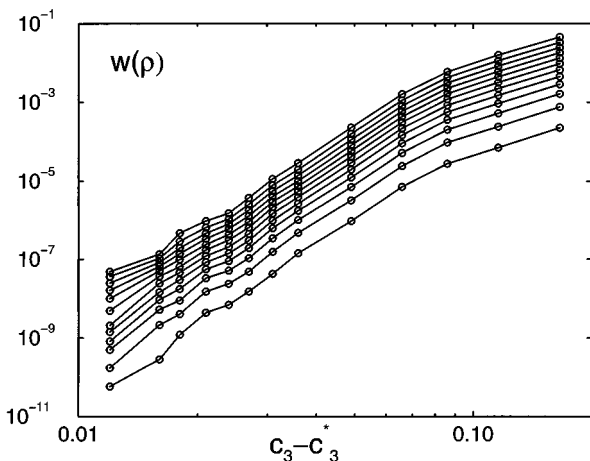


FIG. 5. Log-log plot showing the probabilities to find an amplitude  $< \rho$  against  $c_3 - 0.734$ . Each curve corresponds to a fixed value of  $\rho$ , with  $\rho = m/20$  for the  $m$ th curve from the bottom.

tion of local phase gradients  $\nu_{\text{loc}}$  should decay as  $P(\nu_{\text{loc}}) \sim \nu_{\text{loc}}^{-3}$  (here we assume that  $\nu_{\text{loc}} \sim 1/\rho$  for large  $\nu_{\text{loc}}$ ), in qualitative agreement with observations in [3]. As pointed out in [3,9], the creation of a defect can be similar to a noise-induced widening of an attractor. This would naturally lead to a defect density that decreases exponentially with  $c_3$  [22]. But we believe that the phenomenon looks more like an (interior) crisis [24]. It is known that crises can lead to power laws with very large exponents [25] or even to characteristic time scales that increase faster than any (inverse) power of the distance from the critical point [26]. But it seems that little is known about crises in spatially extended systems [27]. The simplest possibility would be that for each pair  $(c_1, \nu)$  there is a critical circle  $|A| = \rho^*$ . Once this circle is penetrated, the orbit can come arbitrarily close to the origin, and a defect can develop. Unfortunately, we do not see any hint for such a circle in our data. The next simple scenario would be that there is a rotationally and translationally invariant set of tori  $\rho = \rho^*(x, \psi)$  (each of which individually is not symmetric), such that a defect can appear as soon as the solution is inside any one of these tori. We see no way how to test this scenario.

#### IV. LYAPUNOV ANALYSIS AND STABLE SOLUTIONS

To measure the degree of ‘‘chaos’’ of the solutions with  $\nu \neq 0$  in the PT regime, we measured the maximal Lyapunov exponent  $\lambda$ . In order to estimate  $\lambda$ , we have considered the linearized expression of Eq. (1),

$$V_t = (1 + ic_1)V_{xx} + V - (1 - ic_3)(2|A|^2V + A^2V^*), \quad (21)$$

where  $V(x, t)$  is a complex field and  $V^*$  indicates its conjugate. The exponent  $\lambda$  is given by the expression

$$\lambda = \lim_{t \rightarrow \infty} \frac{\ln[M(t)/M(0)]}{t}, \quad (22)$$

where  $M(t) = \int dx |V(x, t)|^2 \equiv \|V\|_t^2$ . Following the evolution of  $V(x, t)$  in the tangent space [given by Eq. (21)] and estimating the growth rate  $M(t)/M(0)$  over a sufficiently long time a realistic estimation of  $\lambda$  can be obtained. It should be noticed that in order to avoid numerical problems the field  $V$  has been renormalized to  $\|V\|_t = 1$  after each time interval  $t = 25$ . We measured  $\lambda$  for several values of  $c_3$  and for several  $\nu$  values in the interval  $[0, \nu_M]$ . Our data are shown in Fig. 6 for  $c_3 = 0.35, 0.40, 0.60$ , and 0.70. They were obtained from single trajectories spanning between  $1.5 \times 10^5$  and  $6 \times 10^5$  time units. This time systematic differences were seen between different initial conditions [we used again Eqs. (16) and (17)], indicating broken ergodicity even for fixed  $\nu$ . The estimated error bars for each  $\lambda$  are smaller than the observed discrepancies, moreover, the probability distributions  $P(\rho)$ , corresponding to different initial conditions, show noticeable differences. Thus there seem to be several coexisting attractors, with slightly different values of  $\lambda$ . This complicates the situation of course, and it might be responsible for the slight nonmonotonicities seen in Fig. 6.

Apart from these, the most evident feature seen in Fig. 6 is the strong decrease of  $\lambda$  with  $\nu$ . Indeed, it seems that in

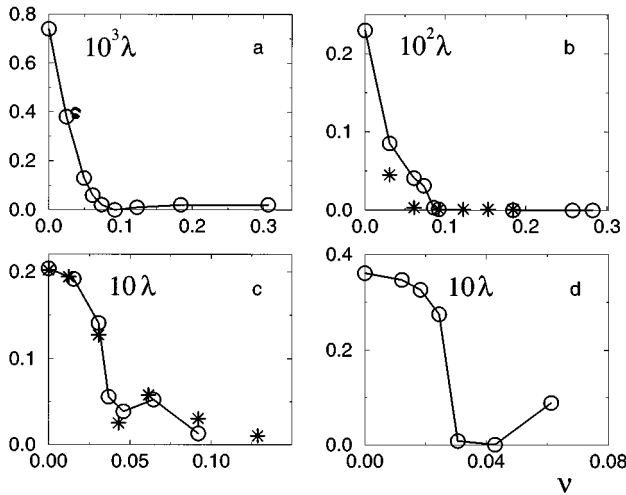


FIG. 6. Maximal Lyapunov exponents  $\lambda$  vs the phase gradient  $\nu$  for  $c_3=0.35$  (a),  $c_3=0.40$  (b),  $c_3=0.6$  (c), and  $c_3=0.7$  (d). Two different sets of initial conditions are considered: Eq. (16) (asterisks) and Eq. (17) (circles). The data have been obtained for system sizes  $L=1024$  and  $2048$  and for integration times  $t=150\,000 - 600\,000$ . For each reported value of  $c_3$ , the maximal estimated error is  $4 \times 10^{-5}$  (a),  $8 \times 10^{-5}$  (b),  $6 \times 10^{-4}$  (c), and  $8 \times 10^{-4}$  (d).

general  $\lambda \rightarrow 0$  for  $\nu \rightarrow \nu_M$ . This decrease is seen even more clearly if averages are taken over several initial conditions, as is done in Fig. 7 for  $c_3=0.5$ . In this figure,  $\lambda$  was averaged over 15–35 trajectories for each value of  $\nu$ , with  $t=10^5$  for each trajectory.

The progressive ordering of the states with increasing  $\nu$  can be directly seen when plotting snapshots of individual solutions. A sequence of such snapshots is shown in Figs. 8 (amplitudes) and 9 (phases). While the configurations seem chaotic for small  $\nu$ , they are more and more regular for larger  $\nu$ , and finally become periodic for  $\nu \approx \nu_M$ . While it is not surprising that the measured  $\lambda$  was zero for Figs. 8(e) and 9(e), it is surprising that the same is also true for Figs. 8(d) and 9(d). Roughly, the latter solution can be described as a sequence of periodic ‘patches’ [each similar to the

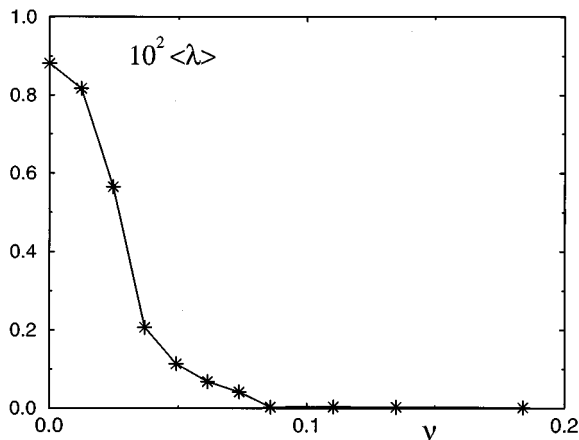


FIG. 7. Maximal Lyapunov exponents  $\langle \lambda \rangle$  for  $c_3=0.5$ , plotted against  $\nu$ . Each value has been obtained by averaging over many initial conditions (from 15 to 35) and over an integration time  $t=100\,000$  for each trajectory. The considered system size is  $L=1024$ .

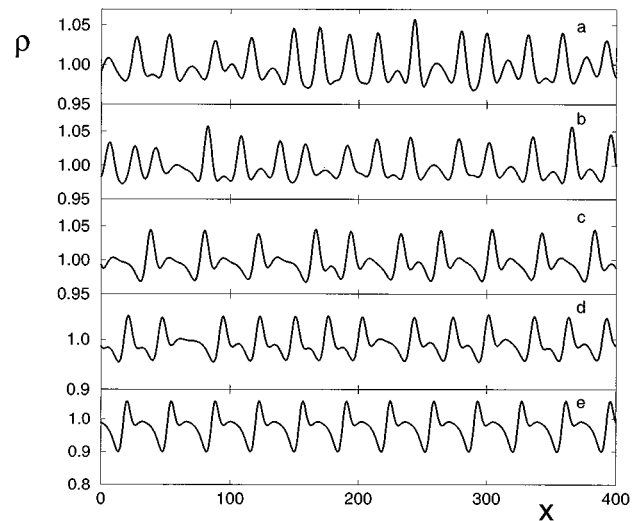


FIG. 8. Amplitude  $\rho(x)$  for  $c_3=0.5$  and for various values of the phase gradient  $\nu$ : 0 (a), 0.01 (b), 0.04 (c), 0.09 (d), and 0.18 (e).

solution shown in Figs. 8(e) and 9(e)], interrupted by ‘faults’ in which the amplitude is nearly constant and the phase decreases linearly.

We have observed such nonchaotic solutions for all  $c_3 \leq 0.5$  when  $\nu \rightarrow \nu_M$ . They can all be expressed in the form

$$A(x,t) = h(x - \nu t) e^{i(\nu x - \omega t)}, \quad (23)$$

where  $h(\xi) = \rho(\xi) e^{i\psi_0(\xi)}$  is in general complex and periodic with period  $L$ . Notice that also its phase is periodic, so that  $\nu$  in Eq. (23) is the total average phase gradient. We found both solutions that are periodic with period  $L$  (forced upon them by the periodic boundary condition) and solutions with smaller period [as, e.g., in Figs. 8(e) and 9(e)]. It is natural to assume that the former would lead to spatially aperiodic solutions for  $L \rightarrow \infty$ . The periodic solutions can be considered as Bloch waves where the periodicity is, however, self-generated and not imposed by some external potential.

Correspondingly, amplitude and phase can be expressed as

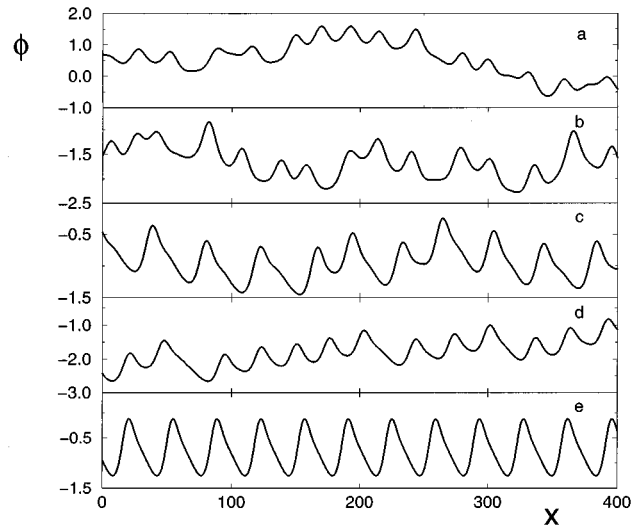


FIG. 9. Same as Fig. 8, but for the phase  $\phi(x)$ .

$$\rho(x,t) = \rho(\xi), \quad \psi(x,t) = \psi_0(\xi) - \omega t + \nu x. \quad (24)$$

where  $\xi = x - vt$ . While the motion of the amplitude is a simple shift with velocity  $v$ , the evolution of the phase is more complicated. At fixed  $\xi$ , i.e., in a coordinate frame moving with velocity  $v$ , the phase increases linearly with  $\partial\psi/\partial t|_{\xi} = v\nu - \omega$ . But there is no fixed phase velocity, i.e., there is no frame in which the phase is strictly constant. It fluctuates around a constant value in a frame moving with velocity  $\langle v_{\text{ph}} \rangle = \omega/\nu$ , which is thus the *average* phase velocity. Typically, we found that  $v$  and  $\langle v_{\text{ph}} \rangle$  are not commensurate. Thus solutions of the type of Eq. (23) display a type of quasiperiodic motion. Similar waves have been found previously in [28,12].

While time-dependent simulations are needed to verify the stability of these solutions, their *existence* can be checked much more easily. Indeed, they are obtained by solving an ordinary differential equation for  $h(\xi)$ ,

$$(1 + ic_1)h_{\xi\xi} + [2i\nu(1 + ic_1) + \nu]h_{\xi} + [1 - \nu^2(1 + ic_1) + i\omega]h - (1 - ic_3)|h|^2h = 0. \quad (25)$$

We should notice that for  $c_3 \geq 0.6$  the picture changes slightly:  $\lambda$  still decreases with  $\nu$ , but nonchaotic solutions are no longer observed.

Another way to simulate regular solutions with periodic  $h(\xi)$  is to use small systems where  $L$  is equal to its period. To obtain arbitrary values of  $\nu$ , we have to use in this case *twisted* boundary conditions  $\rho(x+L) = \rho(x)$ ,  $\psi(x+L) = \psi(x) + \theta$  with a twist  $\theta = \nu L$ . By means of such simulations we checked again the existence of solutions (23). We checked also that there was an upper limit on  $\nu$  that agreed roughly with  $\nu_M$ , though its precise value depended on  $L$ , as one might have expected: depending on its precise value, an integer number of waves will fit into  $L$  with more or less ease.

## V. A MODIFIED KURAMOTO-SIVASHINSKY EQUATION

The behavior of  $\lambda$  as a function of  $\nu$  and the origin of the observed nonchaotic solutions can be explained in the framework of the modified Kuramoto-Sivashinsky equation (MKSE) derived in [6,29]. For completeness, let us recall the main assumptions in deriving the Kuramoto-Sivashinsky equation (KSE) [5,30] and its modification.

It is well known that just above the BF line the amplitude is nearly constant, and its dynamics is essentially ruled by the phase behavior [1]. More precisely, the KSE is obtained by making two main assumptions: first,  $A(x,t)$  is obtained by adding a small perturbation to the spatially constant solution,  $A(x,t) = e^{-i\Omega_0 t} + u(x,t)$ ; and second,  $u(x,t)$  is a ‘‘slaved’’ function of  $\psi(x,t)$  and its spatial derivatives.

In deriving the MKSE we just replace the first assumption by making a perturbation around the plane-wave solution given in Eq. (2). After a tedious and nontrivial calculation [6] one finds that the amplitude is given by

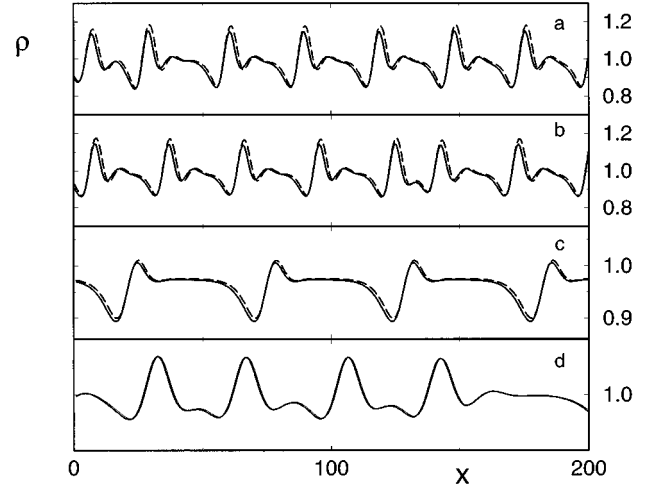


FIG. 10. Amplitudes  $\rho$  from the direct simulation of the CGLE (solid line) and obtained through Eq. (26) (dashed line): (a)  $c_3 = 0.7$  and  $\nu = 0.06$ ; (b)  $c_3 = 0.7$  and  $\nu = 0$ ; (c)  $c_3 = 0.4$  and  $\nu = 0.26$ ; (d)  $c_3 = 0.4$  and  $\nu = 0.03$ .

$$\rho(x,t) = \sqrt{[1 - q(x,t)]^2 + [c_3 q(x,t)]^2} \quad (26)$$

with  $q(x,t) = \{c_1 \partial_x^2 \psi(x,t) + [\partial_x \psi(x,t)]^2\}/2$ , and the phase satisfies

$$\dot{\psi} + \Omega_2^{(1)} \psi_{xx} + \Omega_2^{(2)} (\psi_x)^2 + \Omega_4^{(1)} \psi_{xxxx} + \Omega_4^{(2)} \psi_x \psi_{xxx} = 0, \quad (27)$$

where  $\Omega_2^{(1)} = c_1 c_3 - 1$ ,  $\Omega_2^{(2)} = (c_1 + c_3)$ ,  $\Omega_4^{(1)} = c_1^2 (1 + c_3^2)/2$ , and  $\Omega_4^{(2)} = 2c_1 (1 + c_3^2)$ . Notice that the latter is just the KSE except for the last term.

In order to verify if Eqs. (27) and (26) well approximate the dynamics of the CGLE in the PT regime, two checks have been performed. As a first test, we have evaluated  $\rho(x,t)$  by means of Eq. (26) in the whole PT regime and for several values of  $\nu$ . A comparison with the amplitudes obtained directly from the integration always shows satisfactory results; see Fig. 10. Notice that this is even true for the extremal values  $c_3 = 0.4$  and  $0.7$ , i.e., for two parameter values that are near to the BF line and to the line  $L_1$ .

As a second check, we have derived from Eq. (27) expressions for the amplitude velocity  $v$  and the frequency  $\omega$  associated to the nonchaotic solutions (23). We first observe that the ansatz (23) leads to

$$\omega = -\dot{\psi}(x,t) - \nu \psi'_0(\xi), \quad \partial_x \phi(x,t) = \psi'_0(\xi), \quad (28)$$

where primes indicate derivatives with respect to  $\xi = x - vt$ . We then substitute this into (27) and integrate over all  $x$ . Due to the periodic boundary condition some terms drop out and others can be simplified, leaving us with

$$\omega = \Omega_0 + \Omega_2^{(2)} \langle (\psi'_0)^2 \rangle - \Omega_4^{(2)} \langle (\psi''_0)^2 \rangle, \quad (29)$$

TABLE I. Amplitude velocity  $\nu$  and the frequency  $\omega$  of non-chaotic solutions [see Eq. (23)] for several values of  $c_3$  and  $\nu$ . The first numbers in columns 3 and 4 were obtained from Eqs. (29) and (30), while the directly measured values are given in parentheses.

$c_3$	$\nu$	$\omega$	$\nu$
0.35	0.092	0.317 (0.317)	0.723 (0.726)
0.35	0.184	0.218 (0.218)	1.454 (1.458)
0.35	0.306	-0.021 (-0.021)	2.563 (2.569)
0.40	0.092	0.365 (0.365)	0.731 (0.735)
0.40	0.153	0.305 (0.305)	1.236 (1.241)
0.40	0.282	0.074 (0.070)	2.372 (2.337)
0.50	0.123	0.428 (0.427)	1.256 (1.241)
0.50	0.184	0.355 (0.341)	1.592 (1.650)
0.50	0.245	0.229 (0.223)	1.933 (1.984)

where brackets indicate spatial averages,  $\langle \cdot \rangle = L^{-1} \int_0^L dx$  (a similar result was derived in [29], but with the last term neglected). To obtain an expression for  $\nu$  we multiply both sides of (27) by  $\psi_0'(\xi)$  before averaging, arriving at

$$\nu = \frac{\langle \Omega_2^{(2)}[(\psi_0')^3 + 2\nu(\psi_0')^2] + \Omega_4^{(2)}[(\psi_0')^2\psi_0''' - \nu(\psi_0'')^2] \rangle}{\langle (\psi_0')^2 \rangle}. \quad (30)$$

Numerical tests for several parameter values are shown in Table I. In all cases the agreement between the measured values and the right-hand sides of Eqs. (29) and (30) is very good.

Having verified that Eq. (27) gives a good approximation for the phase dynamics of the CGLE in the whole PT regime, we can now relate our numerical findings to several other observations in the literature. This is again based on an observation by Sakaguchi [29] who noticed that Eq. (27), once  $\psi_x$  is approximated by its average value  $\nu$  in the last term, can be rewritten as an equation for  $s = \psi_x$ :

$$\dot{s} + \Omega_2^{(1)}s_{xx} + 2\Omega_2^{(2)}s s_x + \Omega_4^{(1)}s_{xxxx} + \Omega_3 s_{xxx} = 0, \quad (31)$$

with  $\Omega_3 = \nu\Omega_4^{(2)}$ . This is exactly the so-called Kawahara equation [31,32], which has been studied numerically [31] and theoretically [32,33]. Periodic wave trains formed by pulselike structures have been found in this equation. It has been argued [31] that they are due to the dispersion term  $\propto s_{xxx}$ , a conclusion that was confirmed in a careful analysis by Chang *et al.* [33]. These studies confirm also the coexistence of chaotic and nonchaotic solutions (depending on the initial conditions). Chaotic attractors dominate for small values of the dispersion constant  $\Omega_3$ , while for increasing  $\Omega_3$  periodic attractors prevail. Finally, above a threshold value, only nonchaotic solutions are found. Since  $\Omega_3 \propto \nu$ , our results about the decrease of  $\lambda$  with increasing  $\nu$  and the appearance of wave train solutions for  $\nu \rightarrow \nu_M$  are fully consistent with the findings of [33]. Finally, the observation of Chang *et al.* that stable solutions exist only below a certain threshold — which in our case turns out to be  $\nu \approx 0.1$  for  $0.35 \leq c_3 \leq 0.5$  — explains why no regular solutions were found above  $c_3 = 0.6$ : for  $c_3 > 0.6$ : the value of  $\nu_M$  is below 0.1.

## VI. CONCLUDING REMARKS

In this paper an integration scheme has been introduced that is faster than the usual pseudospectral code at comparable accuracy. It has been successfully employed to study the CGLE in the PT regime for large systems ( $L > 1024$ ) and long integration times ( $t > 10^5$ ). Although we have not applied it to other systems than the CGLE, we believe that it should be useful also for the nonlinear Schrödinger equation and for chemical reaction-diffusion equations.

Particular attention was paid to solutions with nonzero average phase gradient  $\nu$ . For fixed control parameters we always found a maximal conserved phase gradient  $\nu_M$ . It can be used as an order parameter to characterize the PT regime and to describe the transition from phase to defect turbulence: at the transition,  $\nu_M$  vanishes with the mean field exponent. Another order parameter with nonzero values in the DT regime gave the same transition point but another exponent that is more similar to exponents found in previous papers. In contrast, the minimal amplitude values reached in the PT regime do not seem to be useful order parameters, as they are discontinuous at the transition.

For small values of  $\nu$ , the majority of the observed solutions are chaotic. But the maximal Lyapunov exponent typically decreases with  $\nu$ , and stable solutions are more frequent than chaotic ones near  $\nu_M$ . This can be understood by assuming that the phase dynamics is ruled by a modified Kuramoto-Sivashinski equation.

The regular solutions can be either spatially periodic or aperiodic. In both cases they consist of traveling waves whose amplitude and phase velocities are typically incommensurate. These solutions can be considered as generalized Bloch waves with self-generated (periodic or aperiodic) modulation. For spatially periodic regular solutions these results were confirmed by simulations of small systems with twisted boundary conditions [i.e., periodic amplitudes but  $\psi(x+L) = \psi(x) + \theta$ ].

During the final write-up of this paper, we became aware of a paper by Montagne, Hernandez-Garcia, and San Miguel [12] where results similar to those reported in Sec. III have been found. The analysis reported in [12] confirms that  $\nu_M$  can be used as an order parameter in the whole  $(c_1, c_3)$  plane of the CGLE. However, the present paper goes beyond the results of [12] in several aspects. In particular, we have fully characterized the dynamics of solutions with  $\nu \neq 0$  through Lyapunov analyses and the identification of a class of new nonchaotic solutions. Moreover, we demonstrated in detail that traveling wave solutions can be described by a Kawahara equation for their phase, as had been suggested in [12].

## ACKNOWLEDGMENTS

We thank M. San Miguel for sending us Ref. [12] prior to publication, and U. Feudel, E. Hernandez-Garcia, L. Kramer, R. Montagne, and A. Politi for very helpful discussions. One of us (A.T.) was supported by the European Community through Grant No. ERBCHBICT941569, and by the Cooperativa Fontenuova. This work was also supported by the DFG through the Graduiertenkolleg ‘‘Feldtheoretische und numerische Methoden in der Elementarteilchen- und Statistischen Physik,’’ and through SFB 237.

- [1] Y. Kuramoto, *Chemical Oscillations, Waves, and Turbulence* (Springer-Verlag, Berlin 1984).
- [2] M.C. Cross and P.C. Hohenberg, *Rev. Mod. Phys.* **65**, 851 (1993).
- [3] B.I. Shraiman *et al.*, *Physica D* **57**, 241 (1992).
- [4] H. Chaté, *Nonlinearity* **7**, 185 (1994).
- [5] Y. Kuramoto, *Prog. Theor. Phys. Suppl.* **64**, 346 (1978).
- [6] H. Sakaguchi, *Prog. Theor. Phys.* **84**, 792 (1990).
- [7] D.A. Egolf and H.S. Greenside, *Nature* **369**, 129 (1994).
- [8] T. Bohr, E. Bosch, and W. van de Water, *Nature* **372**, 48 (1994).
- [9] D.A. Egolf and H.S. Greenside, *Phys. Rev. Lett.* **74**, 1751 (1995).
- [10] G.L. Lamb, *Elements of Soliton Theory* (Wiley, Toronto, 1980); A.C. Newell, *Solitons in Mathematics and Physics* (SIAM, Philadelphia, 1985).
- [11] P. Manneville, *Dissipative Structures and Weak Turbulence* (Academic Press, San Diego, 1990).
- [12] R. Montagne, E. Hernandez-Garcia, and M. San Miguel, *Phys. Rev. Lett.* **77**, 267 (1996).
- [13] A. Torcini, *Phys. Rev. Lett.* **77**, 1047 (1996).
- [14] W.H. Press *et al.*, *Numerical Recipes* (Cambridge University Press, Cambridge, 1986).
- [15] A. Torcini, H. Frauenkron, and P. Grassberger (unpublished).
- [16] A.D. Bandrauk and H. Shen, *Chem. Phys. Lett.* **176**, 428 (1991).
- [17] K. Takahashi and K. Ikeda (unpublished).
- [18] R.L. McLachlan, *Lect. Appl. Math.* **29**, 325 (1993).
- [19] H. Frauenkron and P. Grassberger, *Int. J. Mod. Phys. C* **5**, 37 (1994).
- [20] H. Frauenkron and P. Grassberger, *J. Phys. A* **28**, 4987 (1995).
- [21] An effective discontinuity in  $\rho_{\min}$  approaching the L1 line has been also observed in [22] for the 1D CGLE and in [23] for the 2D CGLE. But in [23] a decrease of  $\rho_{\min}$  for increasing system size  $L$  and integration time is noticed, and it is speculated that the true minimal value of  $\rho$  might be always zero, in which case there would be no sharp transition between the DT and PT phases. Direct numerical evidence for or against this possibility seems not yet very clear.
- [22] H. Chaté, in *Spatiotemporal Patterns in Nonequilibrium Systems*, edited by P.E. Cladis and P. Palffy-Muhoray (Addison-Wesley, Reading, 1994).
- [23] P. Manneville and H. Chaté, *Physica D* **96**, 30 (1996).
- [24] C. Grebogi, E. Ott, and J.A. Yorke, *Physica D* **7**, 181 (1983).
- [25] J.A. Yorke and E.D. Yorke, *J. Stat. Phys.* **21**, 263 (1979).
- [26] C. Grebogi, E. Ott, and J.A. Yorke, *Phys. Rev. Lett.* **50**, 935 (1983); *Ergod. Theor. Dyn. Syst.* **5**, 341 (1985).
- [27] F. Feudel, U. Feudel, and A. Brandenburg, *Int. J. Bif. Chaos* **3**, 1299 (1993).
- [28] B. Janiaud, A. Pumir, D. Bensimon, V. Croquette, H. Richter, and L. Kramer, *Physica D* **55**, 269 (1992).
- [29] H. Sakaguchi, *Prog. Theor. Phys.* **83**, 169 (1990).
- [30] G.I. Sivashinsky, *Acta Astronaut.* **4**, 1177 (1977).
- [31] T. Kawahara, *Phys. Rev. Lett.* **51**, 381 (1983); S. Toh and T. Kawahara, *J. Phys. Soc. Jpn.* **54**, 1257 (1985).
- [32] T. Kawahara and S. Toh, *Phys. Fluids* **31**, 2103 (1988).
- [33] H-C. Chang, E.A. Demekhin, and D. I. Kopelevich, *Physica D* **63**, 299 (1993).